International Communications in Heat and Mass Transfer 155 (2024) 107533

Contents lists available at ScienceDirect

International Communications in Heat and Mass Transfer

journal homepage: www.elsevier.com/locate/ichmt

Numerical investigation of nanoparticle deposition in a microchannel under the influence of various forces and development of a new correlation

Meng Wang [a,b], Phillip S. Dobson [b], Manosh C. Paul [a,*]

[a] Systems, Power & Energy Research Division, James Watt School of Engineering, University of Glasgow, Glasgow G12 8QQ, UK
[b] Electronics & Nanoscale Engineering Division, James Watt School of Engineering, University of Glasgow, Glasgow G12 8QQ, UK

ARTICLE INFO

Keywords:
Microchannel
Nanofluids
Discrete phase model
Nanoparticle deposition
Electronic cooling system

ABSTRACT

Nanofluid-microchannels have gained prominence in recent years as a means of cooling electronic devices; however, nanoparticle deposition remains a challenge. In this paper, a discrete phase model (DPM) is used to study the effects of various forces on nanoparticle deposition of Al_2O_3-water nanofluids in a straight microchannel. The results indicate that Brownian motion has a significant impact on nanoparticle deposition. For instance, when Cunningham values vary from 1.2 to 0.2, nanoparticle deposition ratios decrease from 8.69% to 3.41%. When the fluid velocity is <0.6 m/s, the thermophoretic force becomes crucial, whereas Saffman's lift force becomes important when the particle diameter is <10 nm. In addition, gravity and pressure gradient forces can be ignored. Virtual mass and drag forces impact deposition indirectly by changing residence times. Finally, a new correlation has been proposed for calculating particle deposition ratios.

1. Introduction

With the development of modern technology, the data that needs to be processed is growing exponentially [1,2]. In the big data era, traditional heat dissipation methods are no longer adequate, and an inefficient cooling system will reduce microelectronic device life [3,4]. During the early 1980s, high latent capacity fluids were considered the best method for the development of coolants [5]. In subsequent decades, Choi et al. [6] introduced the concept of nanofluids, which became novel fluids of ultrahigh thermal efficiency. Nanofluids have been studied for >20 years providing a good understanding of their properties [7], heat transfer rate [8–10], and environmental protection [11]. However, there are very few nanofluid cooling systems available today [12]. The main reason is that nanoparticles are prone to deposit on channel walls due to various forces acting upon them [13].

In parallel, Tuckerman and Pease proposed the concept of microchannels [14]. As a result of their small geometry and low coolant requirements, microchannels can improve both the compactness and performance of cooling devices [15–18]. Despite this, their large surface-to-volume ratio means that, if combined with nanofluids, deposition problems may arise. As a result of many particles colliding with the walls, the nanofluid will lose its high-efficiency properties. Simultaneously, fouling deteriorates microchannel heat transfer, which increases energy consumption and shortens device lifespan [19–21].

Therefore, it is important to investigate the deposition of nanoparticles within microchannels. Nanoparticle deposition has some drawbacks: it reduces the number of nanoparticles in the bulk fluid, which affects the thermophysical properties; nanoparticle deposition also results in increased surface roughness, which reduces the volumetric flow rate of the nanofluid; in the long term, nanoparticle deposition results in abrasion, corrosion, and erosion of microchannels, even resulting in the microchannel becoming completely blocked. The majority of nanoparticle deposition studies focus on stationary fluids and use chemical methods to enhance uniformity and stability. Researchers have considered the chemical reason for it by photographing static nanofluids [22,23]. The addition of surfactants has been identified as one way to obtain stable nanofluids, as surfactants alter the surface properties of the nanoparticles by balancing their net charge [24,25]. Expanding on this work, an investigation was conducted by Manjula et al. [26] to determine the optimal dispersion conditions for aqueous alumina powder suspensions with or without surfactants. Beyond surfactants, mechanical mixing has been employed to maintain nanofluid stability, reducing agglomeration by mechanical stirring or ultrasonication [27–29]. This continually breaks hydrogen and chemical bonds between particles with Rehman et al. [12] finding sonication time affected the average agglomerate size and sediment percentage. However, these studies were all limited to stationary nanofluid depositions.

* Corresponding author.
E-mail address: Manosh.Paul@glasgow.ac.uk (M.C. Paul).

https://doi.org/10.1016/j.icheatmasstransfer.2024.107533

Available online 2 May 2024

Nomenclature

$\overrightarrow{F}$	External body forces
m	Mass
ζ_i	Gaussian white noise function
S_0	Spectral intensity
Δt	Time step
T	Temperature
v	Velocity
k	Thermal conductivity
C_p	Specific heat
k_B	Boltzmann constant
u_B	Nanoparticle Brownian velocity
P	Static pressure
C_c	Cunningham correction
Kn	Knudsen number
d_p	Nanoparticle diameter
D_T	Thermophoretic diffusion coefficient
C_{vm}	Virtual mass factor
τ_r	Particle relaxation time
Re_r	Relative Reynolds number
K	Saffman number
d_{ij}	Deformation tensor
N	Deposition particle number

Greeks

ρ	Density
μ	Dynamic viscosity
ν	Kinematic viscosity
λ	Mean free path
φ	Volume concentration
η	Particle deposition ratio

Acronyms

DPM	Discrete phase model
UDF	User defined function
MAD	Mean absolute deviation

Subscripts

p	Particle
B	Brownian force
T	Thermophoretic force
G	Gravity
V	Virtual mass force
D	Drag force
P	Pressure gradient force
L	Saffman's lift force
nf	Nanofluids
bf	Base fluid

It is also true that the flow field affects nanoparticle deposition, and some researchers have studied the influence of forces on particle deposition during a flow process. Bao et al. [30] studied the characteristics of nanoparticle deposition in a gaseous fluid under various forces and concluded that particle deposition varied under the actions of Brownian, thermophoretic and drag forces. Yin et al. [31] researched aerosol nanoparticle deposition affected by thermophoresis and Brownian motion. They found that Brownian motion is more important for small particles, and thermophoresis caused fewer large particles to accumulate on the ceiling wall. Goudarzi et al. [32] considered nanoparticle migration due to thermophoresis and Brownian motion and reported that thermophoresis is very dependent on volume concentrations, moving nanoparticles to cold walls. On the other hand, Mahdavi et al. [33] simulated a mixed convection pipe flow of Al_2O_3 nanoparticles in water and concluded that relative particle depositions reduced by 28% and 18% respectively if Brownian motion and thermophoresis were omitted. However, these studies focus on gas-based fluids and macro-sized tubes.

In recent years, some researchers have begun to investigate nanofluids in microchannels. Mao et al. [34] developed a new model that includes particle rebound, deposition, and removal in order to predict particle behaviour. According to their findings, the asymptotic value of deposition mass decreased with increasing inlet velocity and decreasing particle concentration. Using CFD-DEM methods, Trofa et al. [35] studied microchannel fouling and quantitatively predicted cluster morphology and growth rate. Jung and Park [36] studied heat transfer phenomena by measuring nanofluid temperature and velocity fields in microchannel heat sinks. It was concluded that the generation rate of thermal entropy was 6.3% lower than that of water. Sarafraz et al. [37] investigated the thermal performance, pressure drop, and thermal fouling resistance parameters of a synthesized Ag/water nanofluid in a microchannel. However, particle deposition in a liquid-based fluid is still limited, and some papers focus on the effect of particle migration on heat transfer [38]. Deposition location and specific deposition surfaces have not been studied in relation to the influence of various forces.

In order to adopt this technology, particle deposition in a nanofluid-microchannel must be resolved, and understanding the effects of various forces on particle motion is a key component. As the majority of existing studies analyse forces on particles moving in a gas-based fluid or a macro-channel, research is needed to understand how various forces

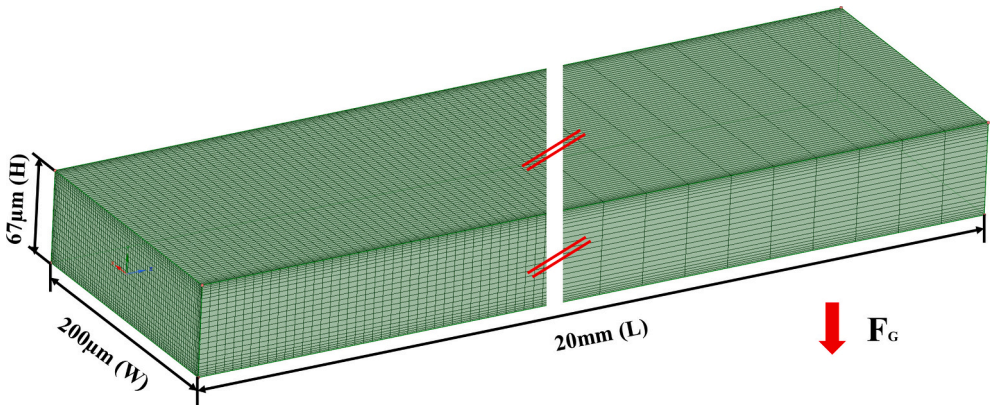

Fig. 1. Diagram depicting the calculation domain and structure of a rectangular microchannel.

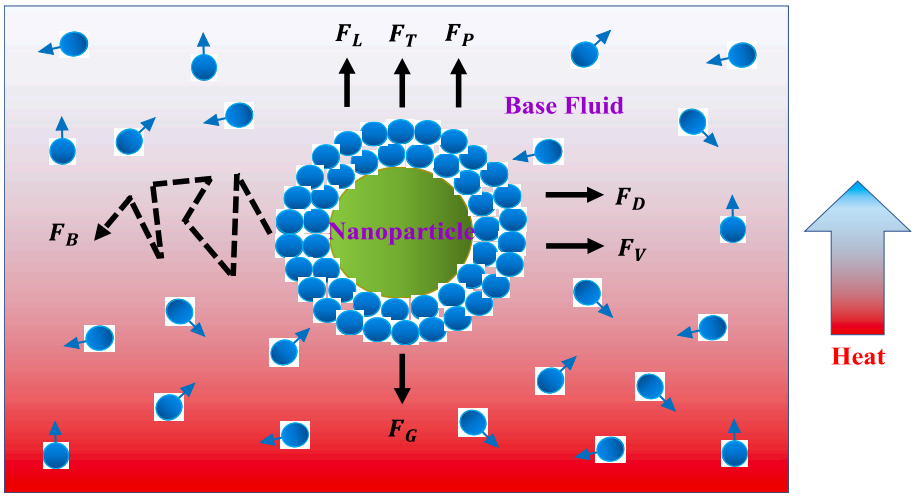

Fig. 2. Schematic of nanoparticle forces near the heated wall.

differ in liquid-based nanofluids and how they cause changes in hydrodynamical factors. Therefore, in this work, DPM and scaling analysis were employed to analyse the influence of various forces on nanofluid deposition in microchannels and compare gas-based and liquid-based fluids to identify strategies to reduce deposition. At the same time, a new correlation was developed to predict particle deposition ratios without the need for a full set of numerical simulations.

2. Numerical methods

The geometry and simulation methodologies used in the paper are the same as those used in our previous work [39]. This section provides a brief introduction.

2.1. Geometry

As shown in Fig. 1, a 3D model of a microchannel having a rectangular cross-section with a width of 200 μm and a height of 67 μm was employed. The microchannel length was 20 mm, which ensured that the flow was fully developed. The structural grid was used in this model to perform inlet densification where the gradient of the flow parameter changes dramatically. For the purpose of evaluating nanoparticle deposition on the walls, a refined near-wall grid density was necessary. Thus, the mesh consists of a first cell with non-dimensional height ($y^+ < 1$).

2.2. Flow field and particle transport simulation

The flow field, governed by the mass continuity, momentum, and energy equations, was simulated using the Discrete Phase Model (DPM) and implemented on ANSYS-Fluent 2020 *Ra*. According to Newton's Second Law of Motion, particle transport is determined by Brownian motion, Saffman's lift force, gravity, thermophoresis, virtual mass force, drag force and pressure gradient force [34,40]:

$$m_p\frac{d\overrightarrow{u_B}}{dt} = \overrightarrow{F_B} + \overrightarrow{F_T} + \overrightarrow{F_G} + \overrightarrow{F_V} + \overrightarrow{F_D} + \overrightarrow{F_P} + \overrightarrow{F_L} \tag{1}$$

Where m_p is the mass of particles; and $\overrightarrow{u_B}$ is the velocity of particles. The various force components of nanoparticles with directions are shown in Fig. 2.

The amplitude of Brownian motion components F_{B_i} is defined as [41,42]:

$$F_{B_i} = m_p\zeta_i\sqrt{\frac{\pi S_o}{\Delta t}} \tag{2}$$

Where ζ_i is the Gaussian white noise function; S_0 is the spectral intensity; and Δt is the time step expressed as:

$$S_0 = \frac{216\nu k_B T}{\pi^2\rho d_p^5\left(\frac{\rho_p}{\rho}\right)^2 C_c} \tag{3}$$

Where k_B is the Boltzmann constant, and C_c is the Cunningham correction that corrects the particle surface conditions expressed as [43]:

$$C_c = Kn\left(0.4exp\left(-\frac{1.1}{Kn}\right) + 1.257\right) + 1 \tag{4}$$

Where $Kn = 2\lambda/d_p$ is the Knudsen number; ν is the kinematic viscosity; d_p is the particle diameter; and λ is the mean free path.

The thermophoretic force is formulated as [44]:

$$\overrightarrow{F_T} = -D_T\frac{\nabla T}{T} \tag{5}$$

Where ∇T is the temperature difference; and D_T is the thermophoretic diffusion coefficient expressed as:

$$D_T = \frac{6\pi d_p\mu^2 C_s(K + C_t Kn)}{\rho(1 + 3C_m Kn)(1 + 2K + 2C_t Kn)} \tag{6}$$

Where $K = k/k_p$.

The virtual mass force is defined as [40]:

$$\overrightarrow{F_V} = C_{vm}m_p\frac{\rho}{\rho_p}\left(\overrightarrow{u_p}\nabla\overrightarrow{u} - \frac{d\overrightarrow{u_p}}{dt}\right) \tag{7}$$

Where C_{vm} is the virtual mass factor.

The Gravity is defined by:

$$\overrightarrow{F_G} = m_p\frac{\overrightarrow{g}(\rho_p - \rho_l)}{\rho_p} \tag{8}$$

Fluid friction is responsible for the drag force, which is determined by [45]:

$$\overrightarrow{F_D} = m_p\frac{\overrightarrow{u} - \overrightarrow{u_p}}{\tau_r} \tag{9}$$

Where τ_r is the particle relaxation time given by:

$$\tau_r = \frac{\rho_p d_p^2}{18\mu}\frac{24}{C_c\,Re_r} \tag{10}$$

Where Re_r is the relative Reynolds number determined by:

Table 1
Specific thermophysical properties.

	ρ [kg/m^3]	c[J/kgK]	k[W/mK]	μ[kg/ms]
Al_2O_3	3880	733	36	/
Water	998.2	4182	0.587	0.000993

$$Re_r = \frac{\rho d_p \left|\overrightarrow{u} - \overrightarrow{u_p}\right|}{\mu} \tag{11}$$

The pressure gradient force is defined as [40]:

$$\overrightarrow{F_P} = m_p \frac{\rho}{\rho_p} \overrightarrow{u_p} \nabla \overrightarrow{u} \tag{12}$$

Lastly, Saffman's lift force is defined by [42,46]:

$$\overrightarrow{F_L} = m_p \frac{2K v^{\frac{1}{2}} \rho d_{ij}}{\rho_p d_p (d_{lk} d_{kl})^{\frac{1}{4}}} \left(\overrightarrow{u} - \overrightarrow{u_p}\right) \tag{13}$$

Where K is the Saffman number, and d_{ij} is the deformation tensor.

DPM divides similar nanoparticles into several small packs, and the position of each pack is determined by tracking a single representative nanoparticle. The number of packs depends on the inlet meshes, and the nanoparticle deposition is evaluated by the deposition ratio as:

$$\eta = \frac{N_d}{N_{total}} \times 100\% \tag{14}$$

Where N_d denotes the number of packs that have been deposited; and N_{total} refers to the total number of packs left from the microchannel's inlet (1875 packs in this case).

The mean absolute deviation (MAD) is used to analyse the differences between data defined as:

$$MAD = \frac{1}{N} \sum_{i=1}^{N} |\eta_1(i) - \eta_2(i)| \tag{15}$$

2.3. Thermophysical properties of nanofluids

Both homogeneous and multiphase models accurately estimate the thermal fields of the diluted nanofluids at low Reynolds numbers [47,48]. According to the homogeneous nanofluid model, the thermophysical properties of nanofluids are determined by the properties of nanoparticles, the base fluid, the temperature, and the concentration of nanoparticles. The thermophysical properties of Al_2O_3 and water are shown in Table 1. The density ρ_{nf} and specific heat capacity $C_{p,nf}$ of Al_2O_3-water nanofluids are determined by nanoparticle concentration φ and defined respectively as [49]:

$$\rho_{nf} = (1-\varphi)\rho_{bf} + \varphi\rho_p \tag{16}$$

$$\left(\rho C_p\right)_{nf} = (1-\varphi)\left(\rho C_p\right)_{bf} + \varphi\left(\rho C_p\right)_p \tag{17}$$

The dynamic viscosity μ_{nf} of Al_2O_3-water nanofluid is given as [50]:

$$\frac{\mu_{nf}}{\mu_{bf}} = exp\left(\frac{4.91\varphi}{0.2092 - \varphi}\right) \tag{18}$$

While the thermal conductivity k_{nf} of Al_2O_3-water nanofluid is shown as [51]:

$$\frac{k_{nf}}{k_{bf}} = 1 + 4.4 Re_p^{0.4} Pr_{bf}^{0.66} \left(\frac{T}{T_{fr}}\right)^{10} \left(\frac{k_p}{k_{bf}}\right)^{0.03} \varphi^{0.66} \tag{19}$$

Here, Re_p is the nanoparticles Reynolds number, defined as:

$$Re_p = \frac{\rho_{bf} v_B d_p}{\mu_{bf}} = \frac{2\rho_{bf} k_B T}{\pi \mu_{bf}^2 d_p} \tag{20}$$

Where v_B is the nanoparticle Brownian velocity; T_{fr} is the freezing point of base fluid, $T_{fr} = 273.15$K.

Table 2
Boundary conditions.

	Type	Heat flux [kW/m^2]	Pressure [Pa]	Velocity [m/s]	DPM	Boundary condition
Outlet	Pressure-outlet	/	/	0	Escape	/
Inlet	Velocity-inlet	/	/	0.1–1	Escape	300 K
Bottom	Wall	0 or 100	/	/	Trap	No-slip
Side	Wall	0	/	/	Trap	No-slip
Top	Wall	0 or 100	/	/	Trap	No-slip

2.4. Grid sensitivity tests and verification

As mentioned above, DPM was used to model nanofluid transport in the microchannel with the specific boundary conditions shown in Table 2. Inlet velocity was varied from 0.1 to 1 m/s, which corresponded to the flow Reynolds number ranging between 10.71 and 107.1. Therefore, the flow regime was laminar flow. In this work, the nanoparticle was Al_2O_3, and the base fluid was water with a nanoparticle concentration $\varphi = 1\%, 4\%$. User-defined functions (UDF) were used to calculate nanofluid properties. Our previous paper already described the specific thermophysical properties of this nanofluid [39] which have not been repeated here. The SIMPLE algorithm was introduced in a pressure-based solver, coupling pressure and velocity. The second-order central difference scheme was applied to the diffusion and convective terms of the transport equations. In the converged solutions, residuals were $<10^{-6}$. Grid sensitivity tests were shown in our previous work [39].

After the grid resolution was successfully tested, simulation validation was performed based on flow field and nanoparticle deposition. For the flow field, the average Nusselt number was compared with the data published in the literature for different Reynolds numbers and volume concentrations, as shown in Fig. 3. The present results are in good agreement with the experimental results of Heris et al. [52], as well as the simulation results of Maiga et al. [53], Bianco et al. [54] and Moraveji et al. [47]. The simulated results of the particle deposition rate are also consistent with those of the theoretical results of Gormley and Kennedy [55] and the simulation results of Shi et al. [56] for the nanoparticle diameter below 100 nm, which have already been shown in our previous article [39].

3. Results and discussion

With the model in place, Brownian motion F_B, thermophoresis F_T, Saffman's lift force F_L, gravity F_G, pressure gradient force F_P, virtual mass force F_V and drag force F_D were analysed one by one, according to their unique characters.

3.1. Impacts of Brownian motion

Brownian motion refers to nanoparticles moving in a random manner. As shown in Eqs. (2)–(4), the influence factors of this force include nanofluid temperature, viscosity, particle diameter and Cunningham correction. Among these factors, nanofluid temperature, viscosity and particle diameter also affect other forces, such as thermophoretic force, drag force and Saffman's lift force. There is only one factor that is correlated with Brownian motion alone, and that is Cunningham correction. According to $Kn = 2\lambda/d_p$, the Cunningham correction is further related to the mean free path which is the average distance moved by the nanoparticles between the two collisions. The

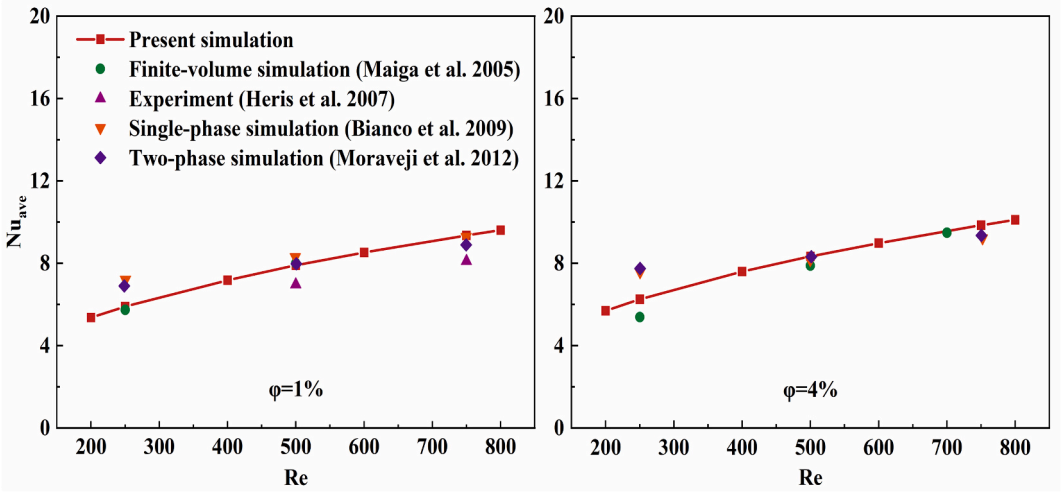

Fig. 3. Nusselt number varies with *Re* at nanoparticle concentrations of 1% and 4%.

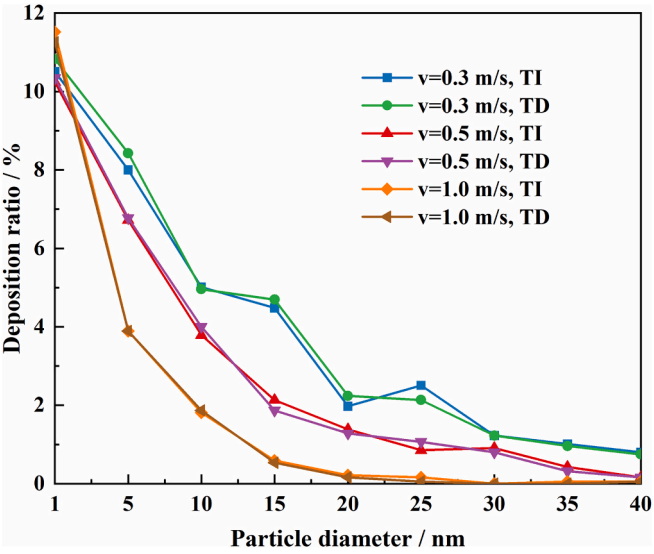

Fig. 4. Deposition ratio varies with particle diameter at the condition of TI and TD.

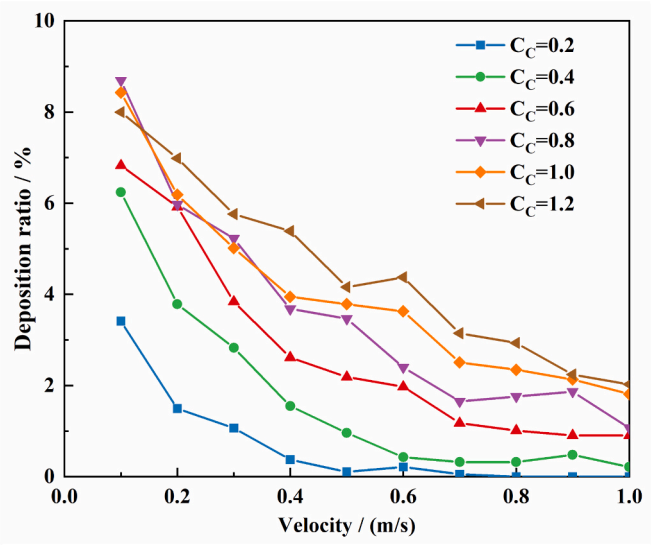

Fig. 5. Deposition ratio changes with fluid velocity in various Cunningham values.

mean free path is therefore considered in how the Brownian force affects particle deposition. The mean free path of molecules in liquid water is about 0.17 nm [57], and the mean free path of molecules in vapour water is about 67.3 nm [58]. According to Eq. (4), considering the same particle diameter, the Cunningham value of gas is higher than the Cunningham value of liquid, which indicates that the Brownian motion in a gas-based fluid is higher than in a liquid-based fluid.

The mean free path is a temperature-dependent (TD) value, but the default DPM set in ANSYS Fluent treats it as a temperature-independent (TI) value. Therefore, it was necessary to investigate how temperature affects this factor when predicting particle deposition. Therefore, the ANSYS coupled UDF routine was used to include TD when calculating the mean free path, and the results between TD and TI were compared. In both cases, the bottom wall of the microchannel was heated at a rate of 100 kW/m^2, whereas the other walls remained adiabatic. Results obtained from three different flow velocities (0.3, 0.5 and 1 m/s) were compared, with the changes in deposition ratio at different particle diameters shown in Fig. 4. The MAD values between TI and TD in the three cases vary only by 0.19%, 0.13% and 0.07%, respectively. It follows, therefore, that the effect of temperature on the mean free path of nanofluids within microchannels can be ignored. This is further explained by the fact that in nanofluids, $Kn << 1$, resulting in $C_c \approx 1$ [59]. Moreover, due to the small size of the particles, the drag force near the wall is equal to that in the bulk fluid, differing from a gas-based mixture [33]. In this regard, the default DPM options are sufficient to define the mean free path for nanofluids in microchannels. The gas-based mixture, however, as emphasised, cannot be used directly.

Additionally, in Eq. (4), the Cunningham value is derived from the mean free path, and Fig. 5 illustrates the variation in deposition ratios with fluid velocity at various Cunningham values (0.2, 0.4, 0.6, 0.8, 1 and 1.2) for a nanoparticle diameter of 10 nm. The deposition ratio at the same velocity varies significantly with Cunningham values, indicating that the Brownian force plays an important role in nanoparticle deposition. Moreover, the particle deposition ratio increases with an increase in Cunningham values due to an increase in the Brownian diffusion coefficient ($D_B = k_B T C_c / 3\pi\mu d_p$) [41]. Interestingly, the rate of change in the deposition ratio decreases as the Cunningham value increases. For instance, the MAD value between $C_c = 0.2$ and $C_c = 0.4$ is 1.04%, while between $C_c = 0.8$ and $C_c = 1$ is 0.5%. A decrease in the deposition ratio occurs when the Cunningham value is >0.8, which indicates that Brownian motion plays a limited role. A similar result has been demonstrated where the particle deposition ratio is around zero

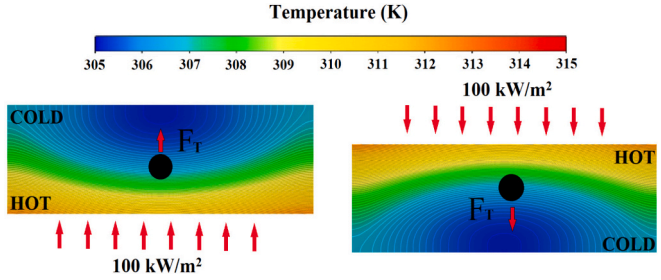

Fig. 6. Temperature contour of two heating conditions with the direction of thermophoretic force.

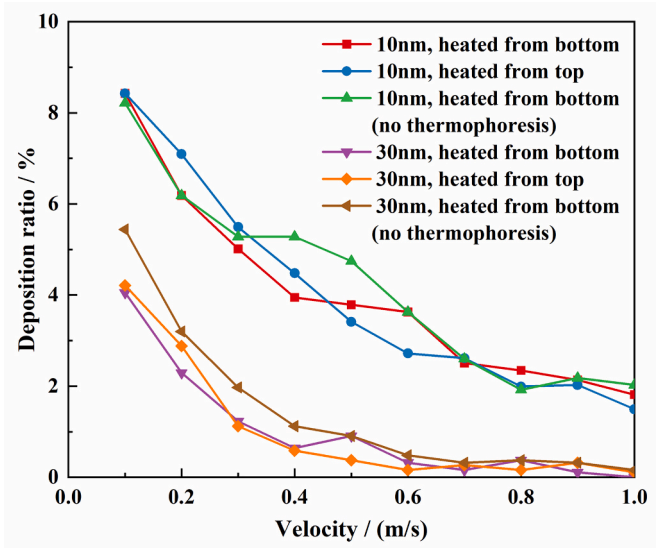

Fig. 7. Deposition ratio changes with velocity for different thermophoretic forces.

when the Cunningham value is 0.2 and the velocity exceeds 0.5 m/s. Therefore, Brownian motion has a great influence on particle deposition.

3.2. Heating directions affecting thermophoretic force

Thermophoresis occurs in suspended particles within nanofluids, and this force causes particles to move from a hot region (high energy) to a cold region (low energy) according to the fluid temperature and temperature gradient. Changing temperature affects Brownian motion, so it is difficult to separate this phenomenon from Brownian motion. As a result, changing the direction of the thermophoretic force was employed to determine the effect of this force, as shown in Fig. 6. Heating from the bottom wall causes the thermophoretic force to point upward, whereas heating from the top wall leads this force to point downward. It has no effect on particle deposition if there is no difference in deposition number; otherwise, it has an effect. Therefore, two cases were simulated, one with a heat flux of 100 kW/m^2 on the bottom wall and the other with the same flux on the top wall.

In Fig. 7, the deposition ratios resulting from the two thermophoretic force directions were compared with no thermophoretic force at different velocities and particle diameters. As shown, when fluid velocities are lower than 0.6 m/s, the deposition ratios are different; but when higher than 0.6 m/s, the deposition ratios are almost the same. For example, for a nanoparticle diameter of 30 nm, as the velocity is lower than 0.6 m/s, MAD = 0.31%; whereas as the velocity is higher than 0.6 m/s, MAD = 0.16%. Consequently, the thermophoretic force has a marked effect on nanoparticle deposition in low-velocity fluids but has little influence in high-velocity fluids due to the fact that low-velocity

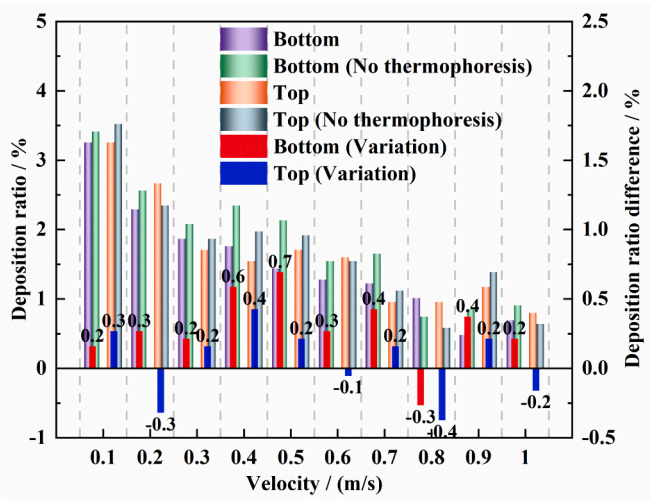

Fig. 8. The deposition ratio varies with velocity at different positions within the microchannel.

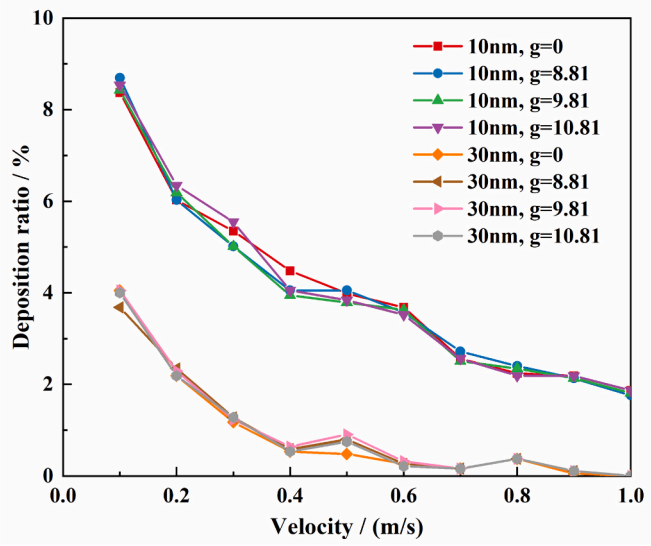

Fig. 9. Deposition ratio changes with velocity at different gravitational accelerations.

fluids have a longer residence time. At the same time, the results of different force directions are also compared, e.g. MAD = 0.41% (10 nm) and MAD = 0.22% (30 nm). In this regard, thermophoresis has a greater impact on small particle diameters than on large particle diameters since small particles have little inertia. Compared with and without thermophoretic force, deposition ratios with thermophoresis are lower than without force at the same velocity and particle diameter. Therefore, the thermophoretic force can reduce deposition effectively.

Fig. 8 illustrates the comparison of specific deposition positions with and without thermophoresis at a particle diameter of 10 nm. At a velocity of 0.1–1 m/s, the MAD is 0.35% on the bottom wall, and the MAD is 0.23% on the top wall. In most cases, the deposition number increases at both the top and bottom positions of the microchannel as thermophoresis is deleted. This consolidates the fact that thermophoretic force prevents nanoparticle deposition. Fig. 7 also supports the same conclusion. It should also be noted that, by turning off the thermophoretic force in ANSYS, the deposition number at the bottom of the microchannel is higher than at the top. The reason for this is that when the wall is heated from below, the direction of the thermophoretic force is upwards. In

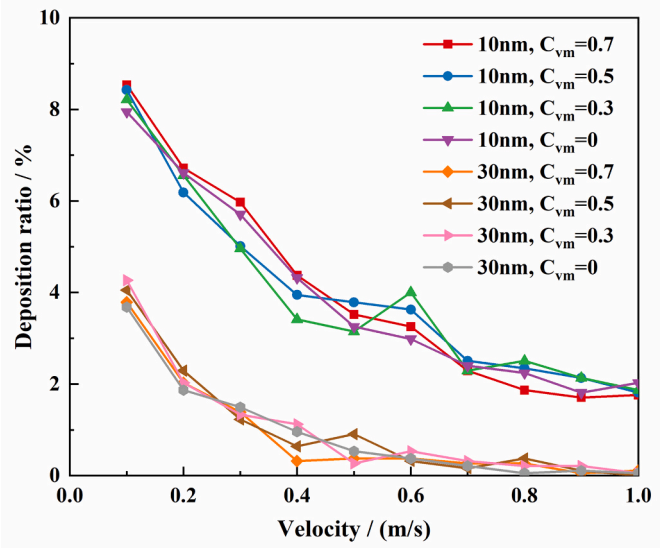

Fig. 10. Deposition ratio changes with velocity at different virtual mass factors.

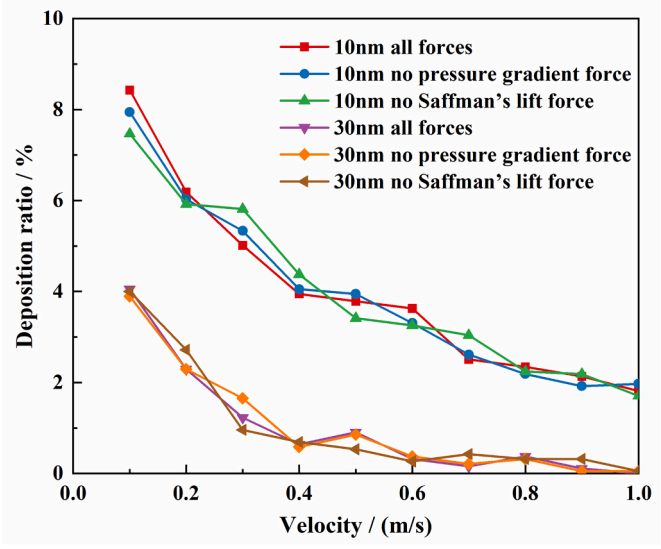

Fig. 11. Deposition ratio varies with velocity at different forces.

addition, this force has a greater influence at low velocity, so the deposition number decreases on the top position at high velocity. All in all, it can be concluded that the thermophoretic force affects particle deposition at low fluid velocity, and it is a resistant force that stops deposition. The main influence factors of this force are nanofluid temperature, temperature difference, nanoparticle thermal conductivity and fluid thermal conductivity, as shown in Eqs. (5) and (6).

3.3. Gravitational field

In order to study the influence of gravity on particle deposition in a microchannel system, gravitational acceleration was altered in the model. Heat flux was maintained at 100 kW/m^2 from the bottom wall with particle diameters of 10 nm and 30 nm. As shown in Fig. 9, the deposition ratio varies with velocity at different gravitational accelerations (0, 8.81, 9.81 and 10.81) m/s^2. In particular, a particle diameter of 10 nm resulted in a maximum MAD of 0.14%, and a particle diameter of 30 nm resulted in a maximum MAD of 0.07%. Fig. 9 shows that the deposition ratio is almost the same regardless of gravitational acceleration. It is, therefore, possible to ignore gravity due to the ultrafine particles and the micro-sized channel used. In this regard, the gravitational field has little effect on particle deposition.

3.4. Virtual mass and drag forces

Virtual mass and drag forces act parallel to fluid flow. The virtual mass force (i.e., added mass) is an inertia-adding force accelerated by the fluid around the particles, and its virtual mass factor is an essential feature of this force. As a result, when particles move in parallel and collide, the virtual mass factor becomes >0.5; whereas when particles move in a line and collide, the factor is <0.5. However, when the concentration of particles is low and particles are far apart, the virtual mass factor equals 0.5 [60]. By changing the virtual mass factors, the influence of virtual mass force was investigated, as shown in Fig. 10. In this case, a heat flux of 100 kW/m^2 was applied to the bottom wall of the microchannel, with particle diameters of 10 nm and 30 nm, resulting in the maximum MADs of 0.24% and 0.15%, respectively. However, particle deposition ratios do not appear to differ across the virtual mass factors for large particles, suggesting that the virtual mass force does not have a significant impact on particle deposition ratios. The reason for this is that the force direction is perpendicular to the direction of deposition. However, there is still some variation, especially for small particles, since it can affect the particle residence time in the flow direction, which indirectly affects deposition ratios. Similarly, drag force has the same effect on deposition as the virtual mass force.

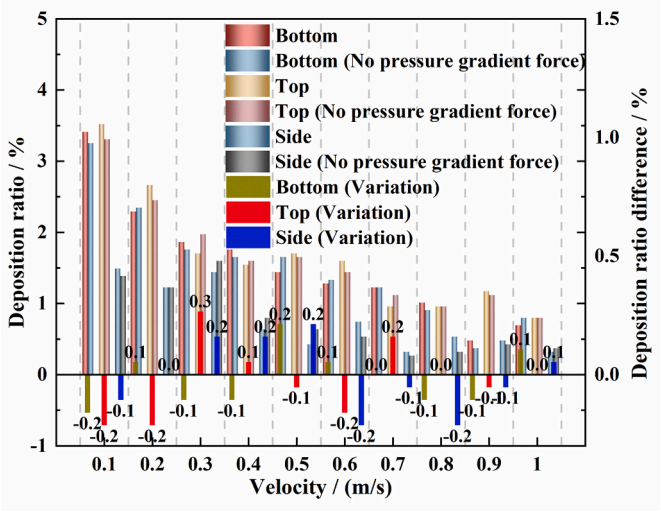

Fig. 12. Deposition ratio changes with and without pressure gradient forces.

3.5. Pressure gradient and Saffman's lift forces

Based on Eqs. (12) and (13), the pressure gradient and Saffman's lift forces are all related to ρ/ρ_p. Consequently, they are negligible when the particle density is much higher than the fluid density. Therefore, in the case of a gas mixture, these two forces are ignored. However, when it comes to nanofluids, their influence is similar to those discussed in the previous sections, making it difficult to distinguish them from other forces. Thus, the simulation was used to compare the results with and without these forces, as shown in Fig. 11. A heat flux of 100 kW/m^2 at the bottom wall of the microchannel remained the same, and the particle diameters of 10 nm and 30 nm resulted in maximum MADs of 0.19% and 0.09%, respectively. Compared with and without pressure gradient forces, the deposition ratios are nearly the same at different velocities. This is because the microchannel is narrow. Therefore, a pressure gradient is unlikely to form. In this case, a slight difference can be attributed to the fact that the heating position changes the density of the base fluid, thereby altering the pressure gradient. The same conclusions

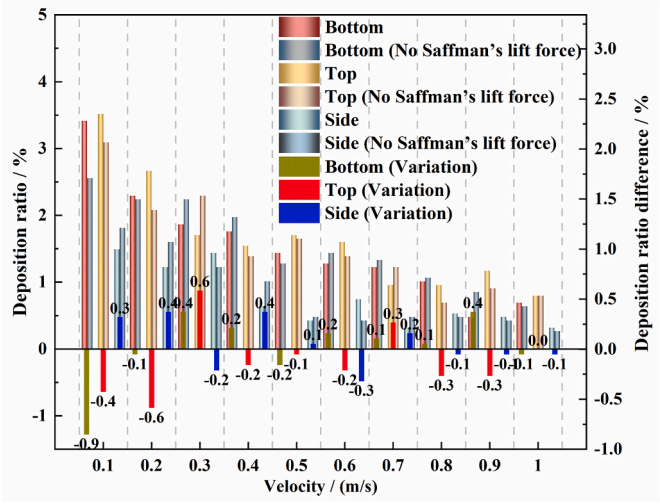

Fig. 13. Deposition ratio changes with and without Saffman's lift forces.

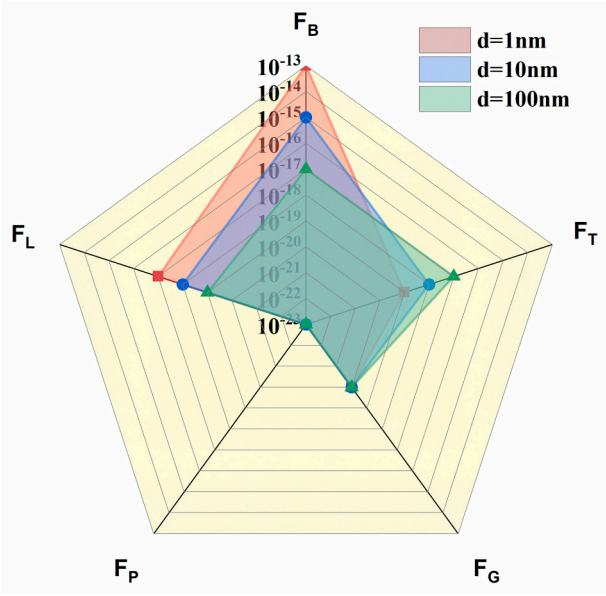

Fig. 14. Magnitude of five forces is calculated in different diameters.

can be drawn from Fig. 12 which shows the MADs of the deposition locations at the bottom, top, and sides are 0.1%, 0.12% and 0.12% respectively.

Saffman's lift force exhibits a different trend from the pressure gradient force. As further shown in Fig. 11, the deposition ratios are almost identical with variation in velocities, compared with and without Saffman's lift force for particles with a diameter of 30 nm (MAD = 0.18%). There is, however, a difference in the deposition ratio when the particle diameter is 10 nm (MAD = 0.4%). As a further analysis of the 10 nm diameter particle, the deposition positions along the microchannel were compared, as shown in Fig. 13. There is a difference in the deposition numbers, especially at the top and bottom walls, which indicates that Saffman's lift force has some influence on the deposition of small particles. Additionally, this force is directed towards the centreline when particles lag behind fluids, preventing some deposition [61]. The influence factors are particle diameter, fluid density, particle density, particle mass, fluid kinematic viscosity and fluid velocity, as shown in Eq. (13).

Table 3
Evaluating the importance of forces in different base fluids.

Force	Liquid-based fluid	Gas-based fluid [8,30]
F_B	Great impact	Great impact
F_T	Medium impact	Little impact
F_G	Little impact	Little impact
F_V	Fluid flow direction	Fluid flow direction
F_D	Fluid flow direction	Fluid flow direction
F_P	Little impact	Little impact
F_L	Medium impact	Little impact

3.6. Scaling analysis

In order to further analyse the importance of all the force components, a scaling analysis of F_B, F_T, F_G, F_P and F_L was calculated according to Eqs. (2), (5), (8), (12) and (13). However, it should be noted that since the virtual mass force and drag force have the same direction as the fluid flow, these two forces are not analysed here. The required scaling includes: $\mu \sim 10^{-3}$, $d_p \sim 10^{-8}$, $k \sim 1$, $k_p \sim 10$, $K_n \sim 10^{-2}$, $\rho \sim 10^3$, $\rho_p \sim 10^3$, $d_{ij} \sim 10^{-2}$, $\vartheta \sim 10^{-6}$, $m_p \sim 10^{-21}$, $T \sim 10^2$, $\Delta T \sim 10$ and $k_B \sim 10^{-23}$. The magnitude of each force was calculated for particles with diameters of 1 nm, 10 nm and 100 nm, as shown in Fig. 14. For nanoparticles below 100 nm, Brownian motion dominates the direction and velocity of nanoparticle motion. Gravitational and pressure gradient forces have a relatively small magnitude and do not change with nanoparticle diameter, making them negligible. The magnitude of thermophoretic and Saffman's lift forces is in the middle, and their impact depends on the diameter of the nanoparticle.

Overall, Brownian motion greatly affects particle deposition in nanofluids flowing in a microchannel, while thermophoretic force and Saffman's lift force have a modest impact, particularly at a low velocity and a small nanoparticle diameter. Gravity and pressure gradient force can be ignored. Van der Waals and electrostatic forces are neglected as a result of their relatively small contribution [55]. The direction of virtual mass and drag forces differs from the direction of deposition, which has an indirect effect by altering the residence time. It is worth noting that the force impacts of a liquid-based fluid differ from those of a gas-based fluid. Comparative results are shown in Table 3, with differences in the density and mean free path between the two media accounting for the variation.

3.7. Correlation

In the study above, it was found that reducing Brownian motion, increasing thermophoretic forces, and using Saffman's lift forces were effective methods for reducing nanoparticle deposition in microchannels. Specifically, nanoparticle deposition was reduced by modifying the properties of the nanoparticles and the base fluid, as well as the velocity of the fluid. As a result, it is necessary to develop a correlation between Reynolds number, particle diameter and volume concentration in order to determine particle deposition ratios. This method provides the advantage of generating the particle deposition ratio at any given parameter without having to run a complete numerical simulation. Consequently, it reduces the time, cost, and effort that are involved in engineering practice when designing the working conditions for new microchannels.

$$\eta = \left(0.09873 \times 1.00187^{-Re \bullet d_p} + 0.000739569\right) \times 100\% \tag{21}$$

Where d_p is the nanoparticle diameter ($5 \le d_p \le 50$), nm; and Re is the nanofluid Reynolds number ($0 \le Re \le 2300$) given by:

$$Re = \frac{\rho_{nf} v d_h}{\mu_{nf}} = \frac{\left[(1-\varphi)\rho_{bf} + \varphi\rho_p\right] v d_h}{\mu_{bf}} \, exp\left(\frac{0.2092 - \varphi}{4.91\varphi}\right) \tag{22}$$

Where φ is the volume concentration ($\varphi \le 5\%$); v is the fluid velocity, m/s; d_h is the hydrodynamic diameter of the microchannel, m; ρ_{bf} is the

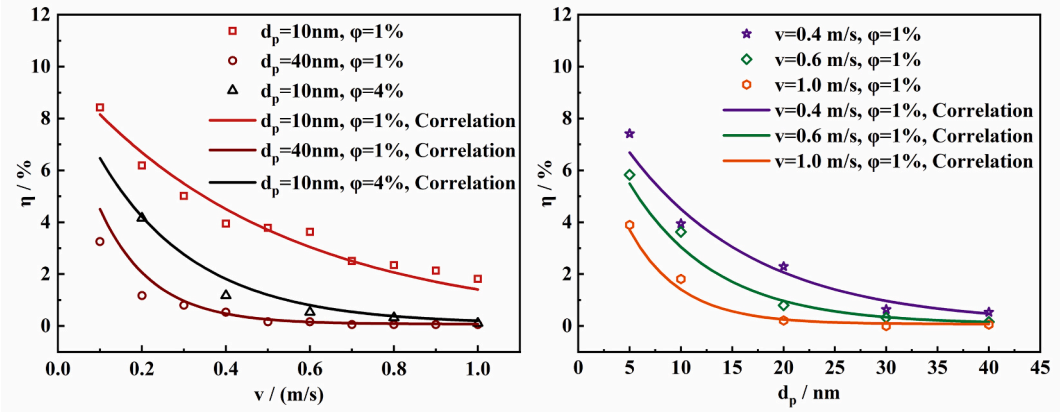

Fig. 15. Validations of the proposed correlations with the numerical results.

base fluid density, m^3/s; ρ_p is the nanoparticle density, m^3/s; and μ_{bf} is the base fluid dynamic viscosity, kg/(ms).

The correlation of Al_2O_3-water nanofluid was developed for the numerical calculation of the particle deposition ratio by using a non-linear regression analysis, as shown in Eqs. (21) and (22). Reynolds numbers, particle diameters and volume concentrations were integral factors in the correlation. R-Square was calculated to be 0.9469. Additionally, Fig. 15 provides a validation between the numerical results and the suggested correlation of particle deposition ratios. It is evident from this figure that the numerical results and the proposed correlation are in good agreement.

4. Conclusion

By using DPM and scaling analysis, this study investigated the influence of various forces on nanoparticle deposition in a microchannel. Several significant findings are as follows:

- Brownian force has the greatest influence on nanoparticle deposition.
- Particle deposition is also affected by Saffman's lift force when the nanoparticle diameter is <10 nm and by thermophoretic force when the fluid velocity is <0.6 m/s.
- The gravitational and pressure gradient forces can be ignored. Virtual mass and drag forces indirectly affect deposition rate by changing particle flow direction residence time.
- Reducing Brownian motion and increasing thermophoretic and Saffman's lift forces are effective methods for reducing nanoparticle deposition in microchannels.
- A new correlation was developed between Reynolds number and particle diameter to determine particle deposition ratios without having to run a complete numerical simulation. This correlation reduces the time, cost, and effort involved in engineering practice.

These conclusions provide some guidance when designing microelectronic cooling devices. Further studies can be conducted using cylindrical particles or other shapes of particles. Moreover, further research is required to determine whether the particle roughness affects the nanoparticle deposition, in order to better implement this new technique for microelectronic cooling applications.

CRediT authorship contribution statement

Meng Wang: Writing – review & editing, Writing – original draft, Visualization, Validation, Software, Methodology, Investigation, Formal analysis, Conceptualization. **Phillip S. Dobson:** Writing – review & editing, Supervision, Resources, Conceptualization. **Manosh C. Paul:** Writing – review & editing, Supervision, Resources, Project administration, Funding acquisition.

Declaration of competing interest

The authors declare the following financial interests/personal relationships which may be considered as potential competing interests:

Meng Wang reports financial support was provided by China Scholarship Council with the University of Glasgow.

Data availability

Data will be made available on request.

Acknowledgements

This work was supported by the China Scholarship Council with the University of Glasgow.

References

[1] J. Wang, M. Evans, M. Belusko, C. Zhao, M. Liu, F. Bruno, Subcooling effect on the optimal performance for a transcritical CO2 heat pump with cold thermal energy storage, Heat Mass Transf. 59 (7) (2023) 1257–1275.
[2] C. Zhao, Y. Sun, J. Wang, K. Hooman, The applicability of volume-averaging method to simulate melting in a multi-scaled periodic structure, Energy 248 (2022) 123636.
[3] M. Wang, R. Zang, E. Hu, A.W. Ezzat, Investigation of air cooler fan start-up delay in liquid refrigerant defrosting system, Appl. Therm. Eng. 143 (2018) 302–307.
[4] M. Bahiraei, S. Heshmatian, Electronics cooling with nanofluids: a critical review, Energy Convers. Manag. 172 (2018) 438–456.
[5] X. Fang, Y. Chen, H. Zhang, W. Chen, A. Dong, R. Wang, Heat transfer and critical heat flux of nanofluid boiling: a comprehensive review, Renew. Sust. Energ. Rev. 62 (2016) 924–940.
[6] H.M. Ali, H. Ali, H. Liaquat, H.T. Bin Maqsood, M.A. Nadir, Experimental investigation of convective heat transfer augmentation for car radiator using ZnO–water nanofluids, Energy 84 (2015) 317–324.
[7] T. Ambreen, M.-H. Kim, Influence of particle size on the effective thermal conductivity of nanofluids: a critical review, Appl. Energy 264 (2020) 114684.
[8] D.-B. Kwak, S.C. Kim, H. Lee, D.Y. Pui, Numerical investigation of nanoparticle deposition location and pattern on a sharp-bent tube wall, Int. J. Heat Mass Transf. 164 (2021) 120534.
[9] X. Yin, C. Hu, M. Bai, J. Lv, An investigation on the heat transfer characteristics of nanofluids in flow boiling by molecular dynamics simulations, Int. J. Heat Mass Transf. 162 (2020) 120338.
[10] X. Liu, D. Toghraie, M. Hekmatifar, O.A. Akbari, A. Karimipour, M. Afrand, Numerical investigation of nanofluid laminar forced convection heat transfer between two horizontal concentric cylinders in the presence of porous medium, J. Therm. Anal. Calorim. 141 (2020) 2095–2108.
[11] H. Gupta, G. Agrawal, J. Mathur, An overview of nanofluids: a new media towards green environment, Int. J. Environ. Sci. 3 (1) (2012) 433–440.
[12] H. Rehman, M. Batmunkh, H. Jeong, H. Chung, Sedimentation study and dispersion behavior of Al2O3–H2O nanofluids with dependence of time, Adv. Sci. Lett. 6 (1) (2012) 96–100.
[13] N.H. Naqiuddin, L.H. Saw, M.C. Yew, F. Yusof, T.C. Ng, M.K. Yew, Overview of micro-channel design for high heat flux application, Renew. Sust. Energ. Rev. 82 (2018) 901–914.

[14] D.B. Tuckerman, R.F.W. Pease, High-performance heat sinking for VLSI, IEEE Electron Device Lett. 2 (5) (1981) 126–129.
[15] J.A. Khan, A.M. Morshed, R. Fang, Towards ultra-compact high heat flux microchannel heat sink, Procedia Eng. 90 (2014) 11–24.
[16] C.A. Rubio-Jimenez, A. Hernandez-Guerrero, J.G. Cervantes, D. Lorenzini-Gutierrez, C.U. Gonzalez-Valle, CFD study of constructal microchannel networks for liquid-cooling of electronic devices, Appl. Therm. Eng. 95 (2016) 374–381.
[17] A. Najafpour, K. Hosseinzadeh, J.R. Kermani, A. Ranjbar, D. Ganji, Numerical study on the impact of geometrical parameters and employing ternary hybrid nanofluid on the hydrothermal performance of mini-channel heat sink, J. Mol. Liq. 393 (2024) 123616.
[18] E. Khodabandeh, S.A. Rozati, M. Joshaghani, O.A. Akbari, S. Akbari, D. Toghraie, Thermal performance improvement in water nanofluid/GNP–SDBS in novel design of double-layer microchannel heat sink with sinusoidal cavities and rectangular ribs, J. Therm. Anal. Calorim. 136 (2019) 1333–1345.
[19] M. Abd-Elhady, C. Rindt, A. Van Steenhoven, Optimization of flow direction to minimize particulate fouling of heat exchangers, Heat Transf. Eng. 30 (10−11) (2009) 895–902.
[20] H. Müller-Steinhagen, M. Malayeri, A. Watkinson, Heat exchanger fouling: mitigation and cleaning strategies, Heat Transf. Eng. 32 (2011) 189–196.
[21] E. Davoudi, B. Vaferi, Applying artificial neural networks for systematic estimation of degree of fouling in heat exchangers, Chem. Eng. Res. Des. 130 (2018) 138–153.
[22] X. Wei, L. Wang, Synthesis and thermal conductivity of microfluidic copper nanofluids, Particuology 8 (3) (2010) 262–271.
[23] X. Li, D. Zhu, X. Wang, Evaluation on dispersion behavior of the aqueous copper nano-suspensions, J. Colloid Interface Sci. 310 (2) (2007) 456–463.
[24] B. Munkhbayar, M.J. Nine, J. Jeoun, M. Bat-Erdene, H. Chung, H. Jeong, Influence of dry and wet ball milling on dispersion characteristics of the multi-walled carbon nanotubes in aqueous solution with and without surfactant, Powder Technol. 234 (2013) 132–140.
[25] X. Li, D. Zhu, X. Wang, N. Wang, J. Gao, H. Li, Thermal conductivity enhancement dependent pH and chemical surfactant for cu-H2O nanofluids, Thermochim. Acta 469 (1–2) (2008) 98–103.
[26] S. Manjula, S.M. Kumar, A. Raichur, G. Madhu, R. Suresh, M. Raj, A sedimentation study to optimize the dispersion of alumina nanoparticles in water, Cerâmica 51 (318) (2005) 121–127.
[27] K.-Y. Kwak, C.-Y. Kim, Viscosity and thermal conductivity of copper oxide nanofluid dispersed in ethylene glycol, Korea-Australia Rheol. J. 17 (2) (2005) 35–40.
[28] M. Kole, T. Dey, Effect of prolonged ultrasonication on the thermal conductivity of ZnO–ethylene glycol nanofluids, Thermochim. Acta 535 (2012) 58–65.
[29] W. Duangthongsuk, S. Wongwises, Comparison of the effects of measured and computed thermophysical properties of nanofluids on heat transfer performance, Exp. Thermal Fluid Sci. 34 (5) (2010) 616–624.
[30] F. Bao, H. Hao, Z. Yin, C. Tu, Numerical study of nanoparticle deposition in a gaseous microchannel under the influence of various forces, Micromachines 12 (1) (2021) 47.
[31] Z.-Q. Yin, X.-F. Li, F.-B. Bao, C.-X. Tu, X.-Y. Gao, Thermophoresis and Brownian motion effects on nanoparticle deposition inside a 90 square bend tube, Aerosol Air Qual. Res. 18 (7) (2018) 1746–1755.
[32] S. Goudarzi, M. Shekaramiz, A. Omidvar, E. Golab, A. Karimipour, A. Karimipour, Nanoparticles migration due to thermophoresis and Brownian motion and its impact on ag-MgO/water hybrid nanofluid natural convection, Powder Technol. 375 (2020) 493–503.
[33] M. Mahdavi, I. Garbadeen, M. Sharifpur, M.H. Ahmadi, J.P. Meyer, Study of particle migration and deposition in mixed convective pipe flow of nanofluids at different inclination angles, J. Therm. Anal. Calorim. 135 (2) (2019) 1563–1575.
[34] S. Mao, T. Zhou, C. Xue, P. Xu, C. Liu, Investigation on fine particle deposition characteristics in narrow rectangular channel based on Eulerian-Lagrangian method, Powder Technol. 420 (2023) 118381.
[35] M. Trofa, G. D'Avino, L. Sicignano, G. Tomaiuolo, F. Greco, P.L. Maffettone, S. Guido, CFD-DEM simulations of particulate fouling in microchannels, Chem. Eng. J. 358 (2019) 91–100.
[36] S.Y. Jung, H. Park, Experimental investigation of heat transfer of Al2O3 nanofluid in a microchannel heat sink, Int. J. Heat Mass Transf. 179 (2021) 121729.
[37] M. Sarafraz, V. Nikkhah, M. Nakhjavani, A. Arya, Thermal performance of a heat sink microchannel working with biologically produced silver-water nanofluid: experimental assessment, Exp. Thermal Fluid Sci. 91 (2018) 509–519.
[38] K.M. Shirvan, M. Mamourian, S. Mirzakhanlari, H.F. Öztop, N. Abu-Hamdeh, Numerical simulation and sensitivity analysis of effective parameters on heat transfer and homogeneity of Al2O3 nanofluid in a channel using DPM and RSM, Adv. Powder Technol. 27 (5) (2016) 1980–1991.
[39] M. Wang, P.S. Dobson, M.C. Paul, Numerical investigation of nanofluid deposition in a microchannel cooling system, Powder Technol. 425 (2023) 118582.
[40] ANSYS Fluent Tutorial Guide, ANSYS, Inc. and ANSYS Europe, Ltd., U.S.A, 2021.
[41] W.C. Hinds, Aerosol Technology: Properties, Behavior, and Measurement of Airborne Particles, John Wiley & Sons, 1999.
[42] A. Li, G. Ahmadi, Dispersion and deposition of spherical particles from point sources in a turbulent channel flow, Aerosol Sci. Technol. 16 (4) (1992) 209–226.
[43] J. Rostami, A. Abbassi, Conjugate heat transfer in a wavy microchannel using nanofluid by two-phase Eulerian–Lagrangian method, Adv. Powder Technol. 27 (1) (2016) 9–18.
[44] L. Talbot, Thermophoresis of particles in a heated boundary layer, J. Fluid Mech. 101 (4) (1979) 737–758.
[45] A. Gosman, E. Loannides, Aspects of computer simulation of liquid-fueled combustors, J. Energy 7 (6) (1983) 482–490.
[46] P. Saffman, The lift on a small sphere in a slow shear flow, J. Fluid Mech. 22 (2) (1965) 385–400.
[47] M.K. Moraveji, E. Esmaeili, Comparison between single-phase and two-phases CFD modeling of laminar forced convection flow of nanofluids in a circular tube under constant heat flux, Int. Commun. Heat Mass Transf. 39 (8) (2012) 1297–1302.
[48] T. Ambreen, A. Saleem, C.W. Park, Homogeneous and multiphase analysis of nanofluids containing nonspherical mwcnt and gnp nanoparticles considering the influence of interfacial layering, Nanomaterials 11 (2) (2021) 277.
[49] Y. Xuan, W. Roetzel, Conceptions for heat transfer correlation of nanofluids, Int. J. Heat Mass Transf. 43 (19) (2000) 3701–3707.
[50] W. Williams, J. Buongiorno, L.-W. Hu, Experimental investigation of turbulent convective heat transfer and pressure loss of alumina/water and zirconia/water nanoparticle colloids (nanofluids) in horizontal tubes, J. Heat Transf. 130 (4) (2008) 042412.
[51] M. Corcione, Empirical correlating equations for predicting the effective thermal conductivity and dynamic viscosity of nanofluids, Energy Convers. Manag. 52 (1) (2011) 789–793.
[52] S.Z. Heris, M.N. Esfahany, S.G. Etemad, Experimental investigation of convective heat transfer of Al2O3/water nanofluid in circular tube, Int. J. Heat Fluid Flow 28 (2) (2007) 203–210.
[53] S.E.B. Maiga, S.J. Palm, C.T. Nguyen, G. Roy, N. Galanis, Heat transfer enhancement by using nanofluids in forced convection flows, Int. J. Heat Fluid Flow 26 (4) (2005) 530–546.
[54] V. Bianco, F. Chiacchio, O. Manca, S. Nardini, Numerical investigation of nanofluids forced convection in circular tubes, Appl. Therm. Eng. 29 (17–18) (2009) 3632–3642.
[55] P. Gormley, M. Kennedy, Diffusion from a stream flowing through a cylindrical tube, in: Proceedings of the Royal Irish Academy. Section A: Mathematical and Physical Sciences, JSTOR, 1948, pp. 163–169.
[56] H. Shi, C. Kleinstreuer, Z. Zhang, C. Kim, Nanoparticle transport and deposition in bifurcating tubes with different inlet conditions, Phys. Fluids 16 (7) (2004) 2199–2213.
[57] K. Takagi, K. Negishi, Measurement of ultrasonic relaxation time and mean free path in liquids, J. Chem. Phys. 72 (3) (1980) 1809–1812.
[58] J.H. Kim, G.W. Mulholland, S.R. Kukuck, D.Y. Pui, Slip correction measurements of certified PSL nanoparticles using a nanometer differential mobility analyzer (nano-DMA) for Knudsen number from 0.5 to 83, J. Res. Nation. Inst. Stand. Technol. 110 (1) (2005) 31–54.
[59] M. Wang, M.C. Paul, P. Dobson, Influence of Brownian motion on nanoparticle deposition in a microchannel heat sink, in: International Conference on Applied Energy, 2021.
[60] A.H. Sulaymon, C.A. Wilson, A.I. Alwared, Experimental determination of the virtual mass coefficient for two spheres accelerating in a power law fluid, J. Fluids Eng. 132 (12) (2010) 121204.
[61] S. Qian, M. Jiang, Z. Liu, Inertial migration of aerosol particles in three-dimensional microfluidic channels, Particuology 55 (2021) 23–34.